Available online at www.sciencedirect.com

ScienceDirect

Geochimica et Cosmochimica Acta 268 (2020) 90–106

Geochimica et Cosmochimica Acta

www.elsevier.com/locate/gca

Control of $CaCO_3$ dissolution at the deep seafloor and its consequences

Bernard P. Boudreau [a,*], Olivier Sulpis [b,1], Alfonso Mucci [b]

[a] Department of Oceanography, Dalhousie University, Halifax, NS B3H4R2, Canada
[b] GEOTOP and Department of Earth and Planetary Sciences, McGill University, 3450 University Street, Montreal, QC H3A 0E8, Canada

Received 24 July 2019; accepted in revised form 20 September 2019; available online 8 October 2019

Abstract

Prediction of the neutralization of anthropogenic CO_2 in the oceans and the interpretation of the calcite record preserved in deep-sea sediments requires the use of the correct kinetics for calcite dissolution. Dissolution rate information from suspended calcite-grain experiments consistently indicates a high-order nonlinear dependence on undersaturation, with a well-defined rate constant. Conversely, stirred-chamber and rotating-disc dissolution experiments consistently indicate linear kinetics of dissolution and a strong dependence on the fluid flow velocity. Here, we resolve these seeming incongruities and establish reliably the kinetic controls on deep-sea calcite dissolution. By equating the carbonate-ion flux from a dissolving calcite bed, governed by laboratory-based nonlinear kinetics, to the flux across typical diffusive boundary layers (DBL) at the seafloor, we show that the net flux is influenced both by boundary layer and bed processes, but that flux is strongly dominated by the rate of diffusion through the DBL. Furthermore, coupling that calculation to an equation for the calcite content of the seafloor, we show that a DBL-transport dominated model predicts lysoclines adeptly, i.e., $CaCO_3$ vs ocean depth profiles, observed across the oceans. Conversely, a model with only sediment-side processes fails to predict lysoclines in all tested regions. Consequently, the past practice of arbitrarily altering the calcite-dissolution rate constant to allow sediment-side only models to fit calcite profiles constitutes confirmation bias. From these results, we hypothesize that the reason suspended-grain experiments and bed experiments yield different reaction orders is that dissolution rates of individual grains in a bed are fast enough to maintain porewaters at or close to saturation, so that the exact reaction order cannot be measured accurately and dissolution appears to be linear. Finally, we provide a further test of DBL-transport dominated calcite dissolution by successfully predicting, not fitting, the in-situ pH profiles observed at four stations reported in the literature.

Keywords: Calcite dissolution; Deep-sea; Dissolution control; Porewater pH; Diffusive boundary layer

1. INTRODUCTION

The dissolution of biogenic $CaCO_3$ at the seafloor is central to controlling the acidity of seawater on time scales of decades to millions of years, and this process figures prominently in creating the geological record of the deep sea (e.g., Kennett, 1982; Broecker and Peng, 1982; Sarmiento and Gruber, 2006; Tyrrell and Zeebe, 2004; Zeebe and Tyrrell, 2019; Boudreau and Luo, 2017; Caves et al., 2016; Boudreau et al., 2018). The current acidification of the oceans, via the absorption of anthropogenic CO_2, will spur transient dissolution of $CaCO_3$ across the seafloor (e.g., Sulpis et al., 2018). Pre-human acidification events have occurred many times in the geological past, as recorded in deep-sea sediments (Zachos et al., 2005; Kump et al., 2009; Zeebe, 2012). The oceans have recovered from these

* Corresponding author.
E-mail address: bernie.boudreau@dal.ca (B.P. Boudreau).
[1] Presently: Geosciences, University of Utrecht, Princetonlaan 8a, 3584 CB Utrecht, the Netherlands.

https://doi.org/10.1016/j.gca.2019.09.037
0016-7037/

acidification events, in large part because of the neutralization capacity afforded by the dissolution of $CaCO_3$ in marine sediments, even if the response time is long by human standards, i.e., up to 10^5 years. Quantitative understanding of the past and future of the oceanic carbonate system requires knowledge of the kinetics of $CaCO_3$ dissolution at the oceanic seafloor.

CO_2-acidified seawater reacts with biogenic $CaCO_3$-tests, overwhelmingly calcite, at the seafloor in a natural version of the human consumption of $CaCO_3$ antacid,

$$CO_2(aq) + CaCO_3 + H_2O \leftrightarrow 2\ HCO_3^- + Ca^{2+}$$

which neutralizes the CO_2 (the excess acid) and constitutes a heterogeneous buffering capacity that is vastly larger, if slower, than available through homogeneous buffering by the dissolved carbonate system (Broecker and Peng, 1982; Sarmiento and Gruber, 2006; Boudreau et al., 2018).

The central role of benthic $CaCO_3$ dissolution in regulating the pH of the oceans has spurred much past research on the kinetics of solid $CaCO_3$ dissolution, particularly of the mineral calcite, in fresh and seawater solutions. These studies can be classified largely within two experimental frameworks: (a) suspended-grain studies and (b) $CaCO_3$-bed dissolution in a chamber with flow. Below, we explain that these two forms of experiments provide fundamentally different information about $CaCO_3$ dissolution kinetics and that care has not always been exercised in applying their results to the seafloor.

Experimental dissolution of suspended calcite grains or spheres in seawater and seawater-like solutions dominates the existing literature. These studies monitor the dissolved carbonate chemistry of a calcite-undersaturated solution with suspended $CaCO_3$ grains/spheres, natural or synthetic, to obtain the rate of dissolution of the mineral as a function of the degree of undersaturation. The degree of undersaturation, 1-Ω (dimensionless), is defined as one minus the ratio of the calcium and carbonate-ion concentration product to the stoichiometric solubility of calcite, K^*, at in-situ temperature and pressure, i.e., $\Omega = [Ca^{2+}][CO_3^{-2}]/K^*$, or $\cong [CO_3^{-2}]/C_s$ in seawater of essentially constant dissolved calcium, where C_s is the carbonate-ion concentration at calcite equilibrium.

Suspension of the calcite grains is employed in an effort to remove the effects of any transport resistance, i.e., diffusion of molecules away from the grains, and thus obtain pure chemical reaction data, i.e., the rate of detachment of ions or molecules from the grain surface. Kinetic rates from dissolving suspended spheres (Peterson, 1966) or calcitic tests (Berger, 1967) have been exclusively interpreted as controlled by mineral-surface reaction rates (Morse and Berner, 1972; Morse and Arvidson, 2002).

The rate of surface dissolution (R_h) from suspended $CaCO_3$ grains has, almost universally, been characterized by a nonlinear dependence on the degree of undersaturation of the surrounding water with respect to calcite $(1 - \Omega)$, e.g., Morse and Berner (1972), Morse (1978), Keir (1980), Maldonado et al. (1992), Arakaki and Mucci (1995), Gehlen et al. (2005a), and Gledhill and Morse (2006). (We do not consider aragonite in this paper, but our analysis would result in the same conclusions.) Most recently, Subhas et al. (2015) have reported high precision experimental dissolution rate measurements as:

$$R_h\left(\text{g cm}^{-2}\text{d}^{-1}\right) = k'_h(1-\Omega)^n \simeq k_h(C_s - C)^n \quad (1)$$

where k'_h is a heterogeneous rate constant (7.2 ± 0.6 g cm^{-2} d^{-1} $= 8.1 \times 10^{-11}$ mol cm^{-2} s^{-1} at 20 °C in seawater), n is the order of reaction, equal to 3.9 ± 0.1 (dimensionless) in these experiments, C is the ambient carbonate-ion concentration in the surrounding fluid, and k_h is an equivalent rate constant (2.6×10^{19} (cm^3/mole)$^{n-1}$ cm s^{-1} at 20 °C), derived from a unit conversion of k'_h at constant seawater calcium concentration. The unit area in Eq. (1) refers to the unit area of reactive surface of a suspended grain.

The fourth order for n is within the range reported by Morse (1978) for natural sediments, but higher than the 2.3 ± 0.4 order observed by Gehlen et al. (2005). A high-order of reaction observed in these suspended-grain experiments indicates that the kinetics of dissolution at the grain surface controls the overall rate, rather than transport limitations to or away from that grain (Morse, 1978; Morse and Arvidson, 2002; Naviaux et al., 2019a,b). The assignment of higher-order kinetics for suspended grains has, however, been challenged by Hales and Emerson (1997), who found a reaction order close to unity after re-examination of the Keir (1980) data. Nevertheless, our current paper questions neither the validity of nonlinear kinetics for suspended calcite grains, nor the values assigned to the reaction order and rate constant.

Based on these suspended grain experiments, diagenetic models have usually represented calcite dissolution in sediments as controlled by nonlinear kinetics within the bed, e.g., Schink and Guinasso (1977), Keir (1982), Archer (1991a,b), Berelson et al. (1994). Such models have often adjusted arbitrarily the calcite-dissolution rate constant to reproduce either observed $CaCO_3$-depth profiles or observed porewater profiles of pH, e.g., Archer et al. (1989), Berelson et al. (1990, 1994), Jahnke et al. (1994, 1997), Martin and Sayles (1996), Hales and Emerson (1997), and Zeebe (2007). This approach frequently led to the conclusion that the rate constant for calcite dissolution in sediment beds was several orders of magnitude smaller than that observed in laboratory experiments – see the summary in Sarmiento and Gruber (2006). This apparent discrepancy has engendered a variety of explanations. Inhibition of dissolution was commonly invoked. Whereas there may well be inhibition of dissolution in natural porewaters, e.g., Morse and Arvidson (2002) and Naviaux et al. (2019a), it is also fair to ask if the large rate constant adjustments in these modelling studies actually constitute a form of repeated confirmation bias: e.g., the kinetics of suspended $CaCO_3$-grain dissolution must be nonlinear, but to explain the seabed pH data, we are free to adjust the high-order rate constant until it reproduces the chosen data, even though the experiments fixed that constant at a much greater value.

What do $CaCO_3$-bed dissolution experiments say about the kinetics? Keir (1983) conducted a study in which a natural deep-sea sediment was spread as a bed across the bottom of a chamber that was stirred overhead by a disk. Keir (1983) interpreted the results of his experiments as

consistent with nonlinear dependency in the degree of undersaturation, as in his suspended grain experiments (Keir, 1980). However, a re-examination of the Keir (1983) experimental data by Boudreau (2013) showed that Keir's dissolution rates were statistically indistinguishable from a first-order dependency on the undersaturation state of the overlaying seawater. This latter finding encouraged Sulpis et al. (2017) to recreate a Keir-like experiment and to demonstrate that the dissolution rate of a calcite bed was not only statistically indistinguishable from first-order with respect to undersaturation, but that it was also dependent on the stirring rate of the overlaying seawater. Regretably, a lack of hydrodynamic theory for the Keir-type reactor limited full interpretation of these results.

At the time of the Keir experiments, Rickard and Sjöberg (1983) and Sjöberg and Rickard (1983, 1984a,b) employed a rotating-disc reactor to study the dissolution of discs and powdered beds of Iceland spar calcite and Carrara marble. In this type of experiment, a disc, containing the sample, rotates at the base of the reactor and there is no overhead stirrer. The motion of the disc causes the fluid in the chamber to flow in a coherent manner, which is described by a well-defined physico-chemical hydrodynamic model – see Sulpis et al. (2019) for particulars on this point. These investigators found that the dissolution rate of such beds remained dependent on the rotation rate for angular velocities up to ~20 rps, which is a relatively fast rotation rate. Furthermore, they found that calcite dissolution appeared to be linear and to follow precisely the rate predicted by the Levich (1962) theory of rotating-disc reactors.

These early rotating-disc results have been largely ignored by the ocean and marine science communities, but they should have raised red flags with respect to seafloor $CaCO_3$ dissolution. Specifically, what these experiments indicated was that $CaCO_3$ dissolution rates at the seafloor could be, in whole or part, controlled by bottom-water hydrodynamics, as current speeds in the deep sea are relatively slow. Low bottom-water speeds create thick diffusive boundary layers (DBL), a layer of water adjacent to the seafloor in which solute transport is dominated by molecular/ion diffusion – see Boudreau and Guinasso (1982) or Boudreau and Jørgensen (2001) for a full

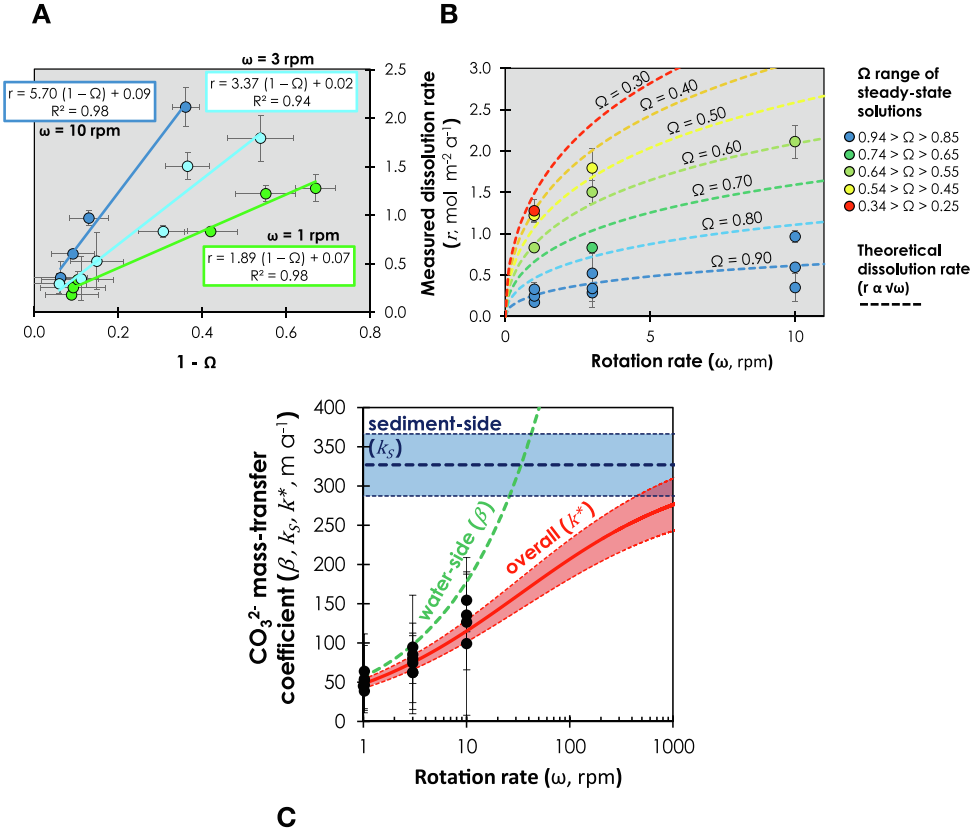

Fig. 1. Plots of the dissolution rate of a calcite bed in a rotating-disc reactor, as obtained by Sulpis et al. (2019). (A) Measured calcite dissolution rates (r) as a function of the steady-state undersaturation state of seawater with respect to calcite ($1 - \Omega$), for three different rotation rates ($\omega = 1$, 3, and 10 rpm, shown in green, turquoise, and blue, respectively). Solid lines are linear regression fits to the data for each rotation-rate. (B) Measured dissolution rate as a function of rotation rate, ω, for different steady-state Ω. Dashed lines indicate the theoretical r values. These results highlight the dominant role of the DBL in controlling the dissolution rate of these beds. (C) A comparison of the experimentally observed mass-transfer coefficients (black dots) with the predicted overall mass-transfer coefficient (k*, solid red line, assuming linear bed kinetics), the sediment-side control limit (k_s, blue dashed line, obtained from Sulpis et al. 2017), and the pure water-side transport control limit (β, the green dashed line), all as a function of the disk rotation rate (ω). Again, $CaCO_3$ bed dissolution is found experimentally to be under mixed control, but water side dominated. (With permission from ASLO and John Wiley & Sons.)

explanation of the DBL. The DBL is much thicker, i.e., on the order of 1 mm (Boudreau and Guinasso, 1982; Santschi et al., 1991; Boudreau, 2001) than boundary layers around suspended individual grains or spheres.

Keeping the above in mind, Sulpis et al. (2019) used a rotating-disk reactor to measure calcite-bed dissolution rates at rotation speeds that produce DBLs of thicknesses of the same order of magnitude as on the deep-sea floor. These experimental results are unequivocal: bed dissolution is linear in undersaturation (Fig. 1A), the overall rate for dissolution follows Levich (1962) transport theory (Fig. 1B), and that rate is largely controlled by transport away from the bed at low rotation speeds (Fig. 1C), matching the conclusions reached by Rickard and Sjöberg (1983). Inescapably, the rate of seafloor calcite dissolution should be subject to the same controls.

Note for clarity: when speaking of control of the dissolution of a bed, we are considering what processes control the overall flux of the solute at the sediment-water interface (SWI). The flux at the SWI is created by the combined effects of the dissolution process in the bed and the diffusion of that solute in the porewater, i.e., the sediment-side transfer rate. That rate is balanced by the rate of diffusion across the DBL that overlies the sediment, i.e., the water-side transfer rate. Whether the flux out of a bed is sediment-side (Fig. 2A), mixed (Fig. 2B), or water-side controlled (Fig. 2C) depends on the relative magnitudes of these transfer rates under the actual natural conditions (geometry, water flow, temperature, etc.). This is something Berner (1978, 1980) largely ignored with his classification of surficial geochemical reactions.

The dissolution of calcite on the seafloor occurs within a porous, but essentially impermeable, bed (Schink and Guinasso, 1977; Takahashi and Broecker, 1977; Boudreau and Guinasso, 1982; Boudreau and Jørgensen, 2001). Within such a sediment, solutes are primarily transported through molecular diffusion, driven by concentration gradients, rather than by the much faster advective transport occurring in stirred reaction chambers. Bioturbation and irrigation are not important players in solute transport in deep-sea porewaters – see Berner (1980), Boudreau (1997), and Burdige (2006). Furthermore, as noted above, a sediment bed is overlaid by a DBL at the SWI. The idea that transport across the DBL influences, if not controls, benthic calcite dissolution at seabeds was initially raised by Pytkowicz (1970) and at first supported by Morse (1974); the concept was then included in early modelling papers by Schink and Guinasso (1977) and Takahashi and Broecker (1977), but generally ignored in many recent papers.

This paper aims to address the inconsistencies detailed above with regard to seabed $CaCO_3$ dissolution. Here, we combine the nonlinear kinetics determined by Subhas et al. (2015), Eq. (1), with transport theory for a seabed to show that:

(a) a mass balance of fluxes indicates water-side-dominated mixed control of seafloor $CaCO_3$ dissolution, and a saturation state of water at the sediment-water interface significantly closer to saturation ($\Omega = 1$) than the value in the overlying waters;
(b) the distribution of the $CaCO_3$ content of sediments with depth in the oceans, i.e., the lysocline, can be explained by a mixed, but water-side dominated, controlled model, but not a sediment-side controlled model. (Our definition of the lysocline contrasts with the definition used by Berger (1968) and Morse and Berner (1972), i.e., a single oceanographic depth where the $CaCO_3$ dissolution rate changes abruptly); and

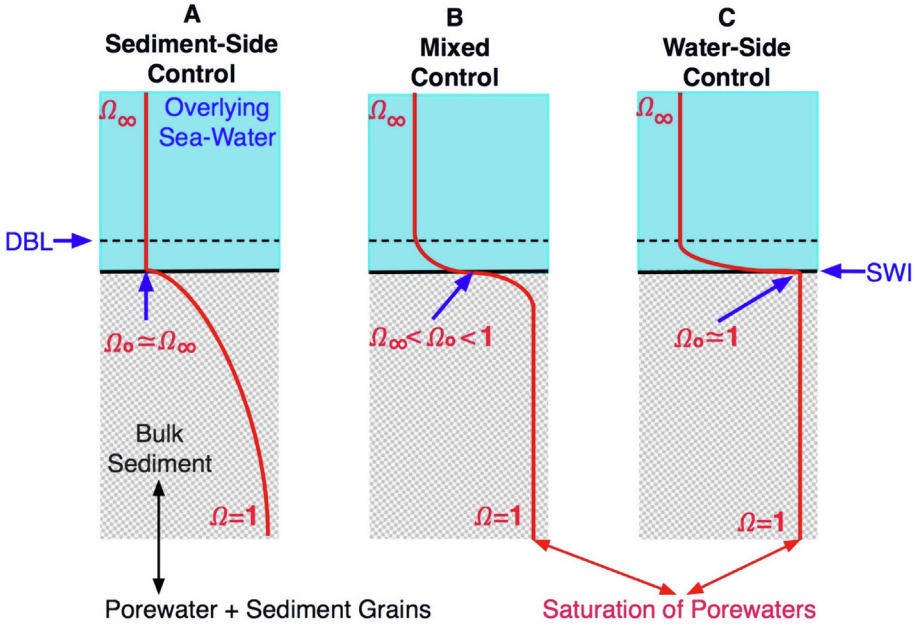

Fig. 2. Schematic diagram of the profile of the carbonate ion, expressed in terms of calcite saturation Ω, within and above the SWI of a deep-sea bed for the cases of (**A**) sediment-side control, (**B**) mixed control, and (**C**) water-side control.

(c) a diagenetic model that assumes water-side-dominated mixed control predicts observed porewater pH profiles, without arbitrary alteration of the kinetic rate constant.

2. INFERRING CONTROL FROM THE FLUX BALANCE

Considerable insight into the controls on $CaCO_3$ dissolution at the seafloor can be obtained simply by considering the flux of the carbonate ion across the SWI. In this analysis, we make a few assumptions that greatly simplify the presentation, without compromising the generality of the results; these are (1) that porosity in the sediment can be treated as constant, (2) that steady state is a reasonable approximation, (3) that the amount of $CaCO_3$ in the sediment is constant with depth in the sediment, i.e., infinitely fast bioturbation of solids (not porewater), (4) that the concentration of the calcium ion can be considered as constant with time and position, all of which are widely assumed in diagenetic modelling (Berner, 1980; Boudreau, 1997; Burdige, 2006), and (5) that only the carbonate ion need be modelled in this section. This last assumption is a bit more problematical, but the results in Boudreau (1987) do not suggest that omission of the other dissolved carbonate species could alter significantly our conclusions.

Under these conditions, the flux of carbonate ions across the DBL, F_{DBL}, must balance the flux of carbonate ions at the SWI created by the $CaCO_3$ dissolution and diffusion of that ion through porewaters, F_S, i.e.,

$$F_{DBL} = F_S \tag{2}$$

The form of F_{DBL} is linear (Boudreau and Jørgensen, 2001)

$$F_{DBL} = -\beta(C_\infty - C_o) \tag{3}$$

where β is the water-side mass-transfer coefficient (Boudreau and Guinasso, 1982), and $\beta = D_{CO3}/\delta$, where D_{CO3} is the (free solution) carbonate ion diffusion coefficient in seawater at in-situ temperature and pressure, δ is the thickness of the DBL, and β has units of a speed (length per unit time). (Please do not confuse the β used here with the β in Dong et al. (2018) or Naviaux et al. (2019a), which has the same units but is the "step kinetic coefficient", an unrelated quantity.) C_o and C_∞ are the concentrations of the carbonate ion at the SWI and in the well-mixed water above the DBL, respectively.

The form of F_S that incorporates nonlinear dissolution kinetics (Subhas et al., 2015) as in Eq. (1), i.e., $n > 1$, was derived by Boudreau and Guinasso (1982; see the Note at that Reference), i.e., their Eq. (6A.15),

$$F_s = -\varphi\left(\frac{2}{5}\right)^{1/2}\left[D'_{CO3}k_c(C_s - C_o)^{n+1}\right]^{1/2} \tag{4}$$

where φ is the porosity of the sediment, D'_{CO3} is the tortuosity-corrected carbonate-ion diffusion coefficient in the porewater (Boudreau, 1997; see the Note at that Reference), C_s is the concentrations of the carbonate ion in equilibrium with calcite, and where

$$k_c = \left(\frac{1-\varphi}{\varphi}\right)k_h\gamma\sigma\rho_{CaCO3}B \tag{5}$$

where k_h is as in Eq. (1), σ is the specific reactive surface area of $CaCO_3$ grains in the sediment (cm^2 per gram), γ is the number of moles per gram of $CaCO_3$ (0.01), ρ_{CaCO3} is the mass density of $CaCO_3$ (g cm^{-3}), and B is the volume of $CaCO_3$ in a unit volume of solid sediment, i.e., the volumetric fraction (dimensionless).

With Eqs. (3) and (4), Eq. (2) now reads as

$$\beta(C_o - C_\infty) = \varphi\left(\frac{2}{5}\right)^{1/2}\left[D'_{CO3}k_c(C_s - C_o)^{n+1}\right]^{1/2} \tag{6}$$

To make our analysis even clearer, let us convert the concentrations to degree of saturation, i.e. $\Omega = C/C_s$, so that Eq. (6) becomes,

$$(\Omega_o - \Omega_\infty) = \frac{k_s}{\beta}(1-\Omega_o)^{(n+1)/2} \tag{7}$$

where

$$k_s = \varphi\left(\frac{2}{5}\right)^{1/2}\left[D'_{CO3}k_c(C_s)^{n-1}\right]^{1/2} \tag{8}$$

The parameter k_s is called the sediment-side mass transfer coefficient (Boudreau and Guinasso, 1982), with units of cm s^{-1}, i.e., again a speed. Note that k_s in Eq. (8) is proportional to the square root of the kinetic rate constant k_h of Eq. (1). A factor of four decrease in k_h, due to inhibition, as advanced by Naviaux et al. (2019a), would be halved in k_s and not alter the essence of the results given below. In addition, we note that experimental values of k_s from real sediments (Keir, 1983; Boudreau, 2013) are statistically indistinguishable from laboratory-derived values with artificial calcite beds (Sulpis et al., 2017) – see Section 4 below.

The ratio k_s/β (dimensionless) in Eq. (7) is a measure of the capacity of the reactive sediment-porewater system to deliver carbonate ions to the SWI (k_s) versus the capacity of DBL transport (β) to move these ions way from the SWI. As the denominator and numerator both have units of speed, the ratio can also be viewed as the speed at which carbonate ions are delivered to the SWI compared to the speed at which they can be removed across the DBL. Consequently, if $k_s/\beta \gg 1$, then DBL transport is slow compared to the release from the sediment and the rate of dissolution is said to be water-side controlled (Fig. 2C); conversely, if $k_s/\beta \ll 1$, the speed of supply from the sediment is much slower than the transport speed across the DBL, and this situation is said to be sediment-side controlled (Fig. 2A). Intermediate values of k_s/β indicate that both water-side and sediment-side processes influence the rate of dissolution and the situation is termed mixed control (Fig. 2B). k_s/β has no name, but resembles a Damkohler number (Boudreau, 1997).

Under water-side control, the balance in Eq. (7) demands that $\Omega_o \simeq 1$, i.e., that the water at the SWI is close to saturation with respect to calcite (Fig. 2C); with sediment-side control, $\Omega_o \simeq \Omega_\infty$, i.e., the saturation of the water at the SWI is close to that of the water above the DBL (Fig. 2A). The mixed case generates Ω_o values between 1 and Ω_∞ (Fig. 2B). Therefore, calculating the

ratio k_s/β and the value of Ω_o for seafloor conditions can inform us about the controls on calcite dissolution in deep-sea sediments.

To obtain k_s/β values, the parameter n in Eq. (7) is set to 4, while the heterogeneous rate constant, k_h from Eq. (1) is reduced by a factor of 4 to obtain its value at an average deep-sea temperature of 2 °C, i.e., equivalent to an activation energy of ~50 kJ mole^{-1} (Sjöberg and Rickard, 1984b; Boudreau, 2013), which is likely too large, as it is double the far-from-equilibrium activation energy of Naviaux et al. (2019b). Porosity is set to 0.8 as typical of deep-sea sediments; D_{CO3} is set to 4.6×10^{-6} cm^2 s^{-1} (Boudreau, 1997), the tortuosity of the sediment is set to 1.6. The specific reactive surface area is set to 6.0×10^4 cm^2 g^{-1}, which is in the center of the range given by Keir (1980) and Subhas et al. (2015) but lower than the average in Gehlen et al. (2005b); the density of the calcite tests is set to 2.5 g cm^{-3}. The mass transfer coefficient, β, below the carbonate saturation depth of the open ocean and away from continents, while variable, is generally in the range of 5–15 m a^{-1} or 1.6–4.1 cm s^{-1} (Boudreau, 2001, 2013; Boudreau et al., 2010a,b), whereas values over 20 m a^{-1} were calculated by Sulpis et al. (2018) over ridges and beneath equatorial currents, but below 5 m a^{-1} in abyssal areas. The 5–15 m a^{-1} range is equivalent to DBL thicknesses (δ) between 0.1 and 0.3 cm, and in this Section, we report the transport condition in our figures at these two limiting δ values.

Neither of the final two parameters, C_s and B, are constants; both are functions of oceanic depth; thus, we report our results as functions of water depth. Carbonate ion concentrations in the bottom waters (C_∞) are computed from GLODAP v2 data (Key et al., 2015; Olsen et al., 2016). Because the computed C_∞ is dependent on the carbonate system pair that is used to compute its value (i.e., total alkalinity and ΣCO_2, total alkalinity and pH, ΣCO_2 and pH, see Millero, 2007; Naviaux et al., 2019a; Raimondi et al., 2019), we computed C_∞ for each of these pairs and used the average. Only samples within 100 m of the bottom were used. Calculations were performed in CO2SYS (Lewis and Wallace, 1998; van Heuven et al., 2011), using GLODAPv2 dissolved inorganic silica and soluble reactive phosphate concentrations, the carbonic acid dissociation constants (K^*_1 and K^*_2) from Lueker et al. (2000) and the HSO_4^- dissociation constant from Dickson (1990). For B values, we use empirical fits to the surficial (0–10 cm) calcite content data from various areas of the oceans (see Part 1 of the Supplementary Information for illustrations of these fits), extracted from dbSEABED (Jenkins, 1997; Goff et al., 2008). C_s is calculated from the equation given by Boudreau et al. (2010a).

2.1. Results

The calculated water-depth distributions of k_s/β and Ω_o are given in Figs. 3 and 4, respectively, for four distinct oceanic regions around the globe, i.e., NW and SW Atlantic, S Indian and Central Equatorial Pacific (C Eq Pacific). These selected regions reflect the range of the dissolved carbonate chemistry observed in the oceans; other adjacent regions provide entirely similar results. The FORTRAN code for these calculations is reproduced in the Supplementary Information (SI, hereafter).

2.2. Discussion

The ratio k_s/β is at all depths and for both DBL thicknesses (1 and 3 mm) far greater than 1, as illustrated in Fig. 3, reaching as high as 750 with the thicker DBL in the SW Atlantic and C Eq Pacific, and never falling below 25 with the thinner DBL in the S Indian. The lowest values of k_s/β occur at the carbonate compensation depth (CCD), defined operationally here as the depth below which the $CaCO_3$ content of the sediment falls to 10%. Over the lysocline in each of the areas, k_s/β is typically between 100 and 700. The interpretation of this result is that water-side processes are as much as 750X slower than the sediment-side processes in all the examined oceanic areas, except nearing the CCD; consequently, water-side processes dominate the mixed control of benthic dissolution in the oceans. This does not mean that sediment-side processes cannot influence deep-sea $CaCO_3$ dissolution, but their importance is restricted to depths near or below the CCD, where k_s/β decreases because of reduced B – see Eq. (5). All this is said without taking into account oxic organic-matter decay, which produces dissolved CO_2 and can lower the saturation state of porewaters. In general, however, organic matter decay occurs on a scale much deeper in sediments than surficial $CaCO_3$ dissolution (see Section 5 below), so that the above conclusion should remain valid.

Water-side dominance is further illustrated by the predicted saturation state at the sediment-water interface, Ω_o, as seen in Fig. 4. Even though the degree of undersaturation in the overlying water, Ω_∞ (red lines), falls as low as 0.66, Ω_o is generally greater than 0.95 through the lysocline and above 0.9 at the CCD, except in the S Indian, where it reaches 0.88. Nonetheless, it is safe to say that Ω_o remains much closer to saturation, $\Omega = 1$, than to Ω_∞, even under the most undersaturated of overlying waters.

3. PREDICTING $CaCO_3$ DEPTH-PROFILES (LYSOCLINES) WITH NONLINEAR KINETICS

As noted above, Morse and Berner (1972) asserted that the dissolution rate of suspended calcite spheres (Peterson, 1966) or suspended forams or coccoliths (Berger, 1967) could only be explained by surface-reaction control, as diffusion rates from these bodies were demonstrably faster. We take no issue with that result. They then stated that the apparent rapid increase in the rate of dissolution in the original Peterson (1966) data at about 3850 m depth in the N Pacific was the result of a nonlinear dependence of the degree of undersaturation ($1 - \Omega$) and that this generated the fall in the $CaCO_3$ content of the sediments below this depth, culminating in the CCD. (The observed changes in the dissolution rate of these suspended $CaCO_3$ experiments with changing saturation state of the ambient seawater may be true, but given the poor quality of the carbonate system data of that time and the uncertainty in the values of K^*_{sp}, we doubt that a definitive pronouncement about nonlinearity could, in reality, have be made.) In addition, Takahashi and Broecker (1977) produced results that indi-

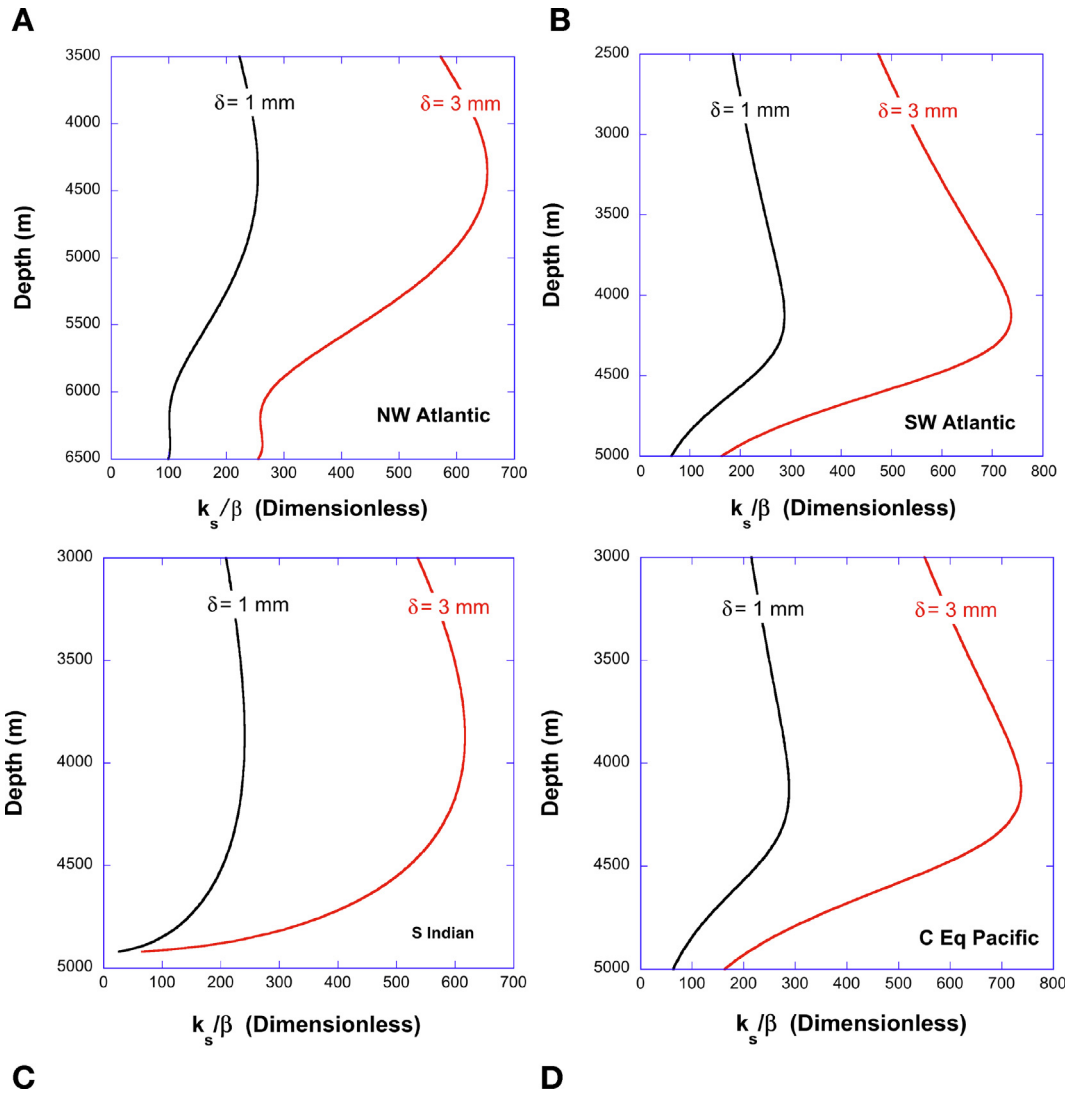

Fig. 3. Plots of the parameter grouping k_s/β (dimensionless) with oceanic depth for 4 typical ocean regions: (**A**) NW Atlantic, (**B**) SW Atlantic, (**C**) S Indian, and (**D**) C Eq Pacific. The two curves in each panel correspond to DBL thicknesses of 1 and 3 mm, spanning the normal range for the deep oceans. Values of k_s/β greater than 1 indicate water-side control of benthic calcite dissolution.

cated that a "stagnant film model", read: water-side controlled model, could not reproduce the lysocline, as it generated no "tail" of low $CaCO_3$ values, as observed in real data. Yet, in the same volume, a model by Schink and Guinasso (1977) generated a tail of $CaCO_3$ with considerable water-side influence; Takahashi and Broecker (1977) may have been a bit too hasty in their conclusion on this point, as argued by Boudreau (2013).

Where Morse and Berner (1972) and Berner and Morse (1974) erred was to extrapolate that the dissolution kinetics of a suspended sphere apply directly to the seafloor. This interpretation of the lysocline then permeated the geochemical and oceanographic literature, further propagated by Berner (1980), Morse (2005), and Morse and Arvidson (2002). As demonstrated by our calculations above, using the modern Subhas et al. (2015) dissolution rates, that assumption is false. In this section, we illustrate that the lysocline is readily reproduced by a model with water-side-dominated mixed control and that a model with only sediment-side control, using the Subhas et al. (2015) rate equation, invariably fails to generate observed lysoclines.

To predict B, rather than use the $CaCO_3$-depth data to fix B as in Section 2 above, Eq. (6) needs to be supplemented. In particular, an equation that accounts for the accumulation of $CaCO_3$ is needed, from which B itself can be calculated. (Note that our logic and approach here are not circular; we do not use the results of the previous section to obtain B; all we employ is Eq. (6), which is of general validity.) The required formula is Eq. (1) in Boudreau (2013), which states that the difference between the flux of calcite to the sediment-water interface, F_B, and the rate of dissolution per unit area, F_D, must equal the accumulation rate of calcite in the sediment, i.e.,

$$F_B - F_D = (1-\varphi) w \rho_{CaCO3} B \tag{9}$$

where (Boudreau, 1997; Boudreau, 2013),

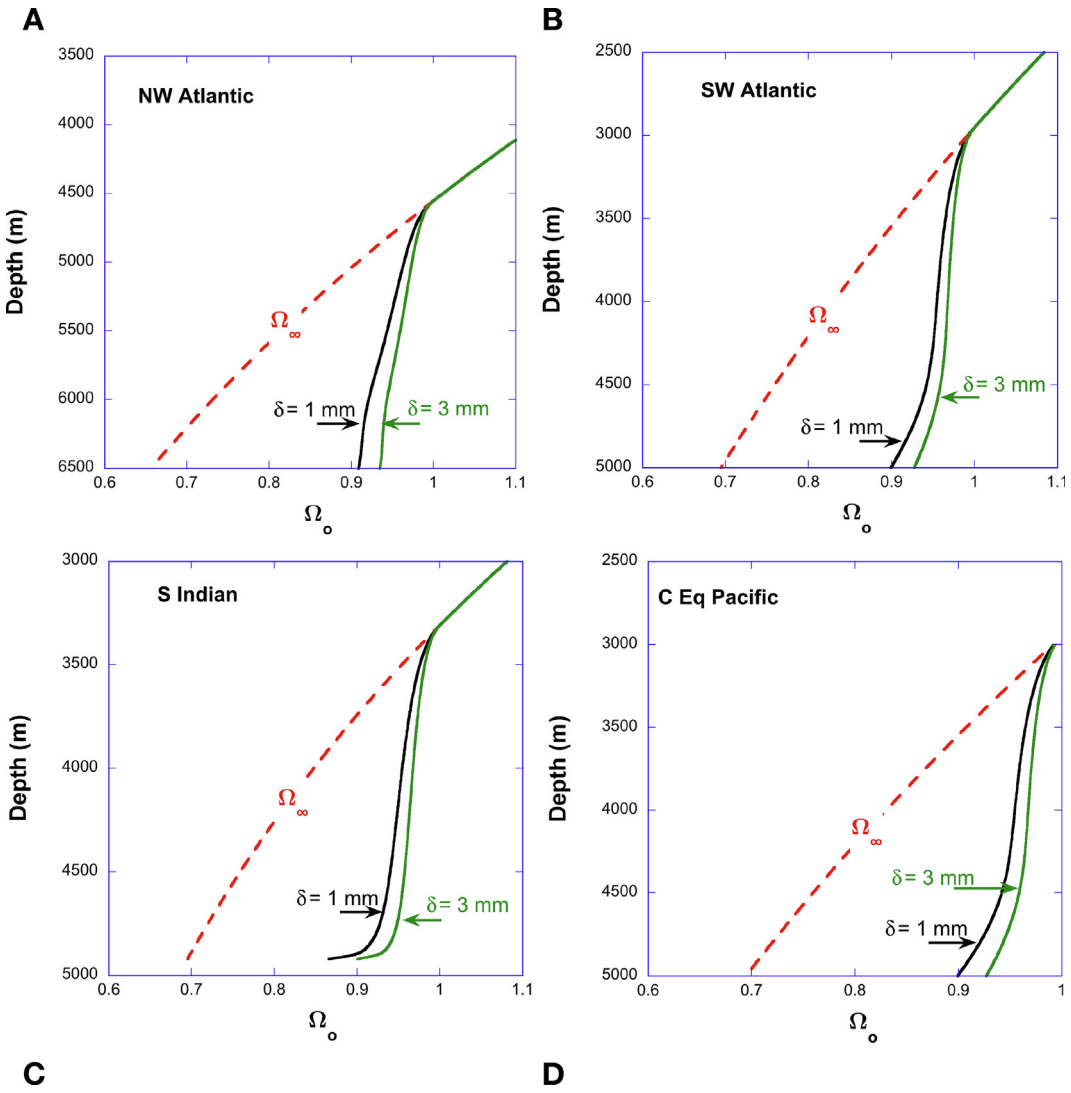

Fig. 4. Plots of the degree of undersaturation of the water at the sediment-water interface as a function of oceanic depth for the 4 same ocean regions as in Fig. 3. Each panel has two curves for Ω_o, one for a DBL thickness of 1 mm (black) and the other for a thickness of 3 mm (green). The saturation of the waters above the DBL (Ω_∞) is also plotted (red curve). Note that Ω_o is distinctly greater than Ω_∞ and remains much closer to saturation at all depths.

$$w = \frac{F_B - F_D}{(1-\varphi)\rho_{CaCO3}} + \frac{F_M}{(1-\varphi)\rho_M} \tag{10}$$

Here, w is the sediment accumulation speed (cm s^{-1}), ρ_{CaCO3} is the mass density of calcite, F_M is the flux of non-carbonate materials (g cm^{-2} s^{-1}), and ρ_M is the mass density of the non-carbonate solids, mostly clay in the deep-sea (~2.5 g cm^{-3}). Combining Eqs. (9) and (10), we obtain,

$$B = \frac{F_B - F_D}{F_B - F_D + \frac{\rho_{CaCO3} F_M}{\rho_M}} \tag{11}$$

which is our desired equation for B.

3.1. Results

In the results illustrated in Fig. 5, F_B and F_M are depth-independent constants and taken to be typical of the selected region of the deep-sea (see Boudreau et al., 2010b). In our calculations, their exact values are varied modestly between regions to reproduce the calcite content observed above the calcite saturation depth, i.e., the oceanic depth where $\Omega = 1$, in each region – see Table S1 of the SI for the exact values employed in this Section. F_D in Eqs. (9)–(11) can be set to either F_{DBL} or F_S, as the choice is arbitrary due to the equality in Eq. (2). Solely for mathematical convenience, F_{DBL} is utilized. The values of β in this section are chosen so as to produce the observed CCD with mixed (nonlinear) kinetics within the chosen region of the oceans – see Table S1; these β values are largely within the range used in Section 2, but three values are below the stated range (thicker DBLs) and one is above (thinner DBL). This variability should not be a cause for concern; ocean currents are spatially (and temporally) variable, and the deviations do not change the conclusions of the pre-

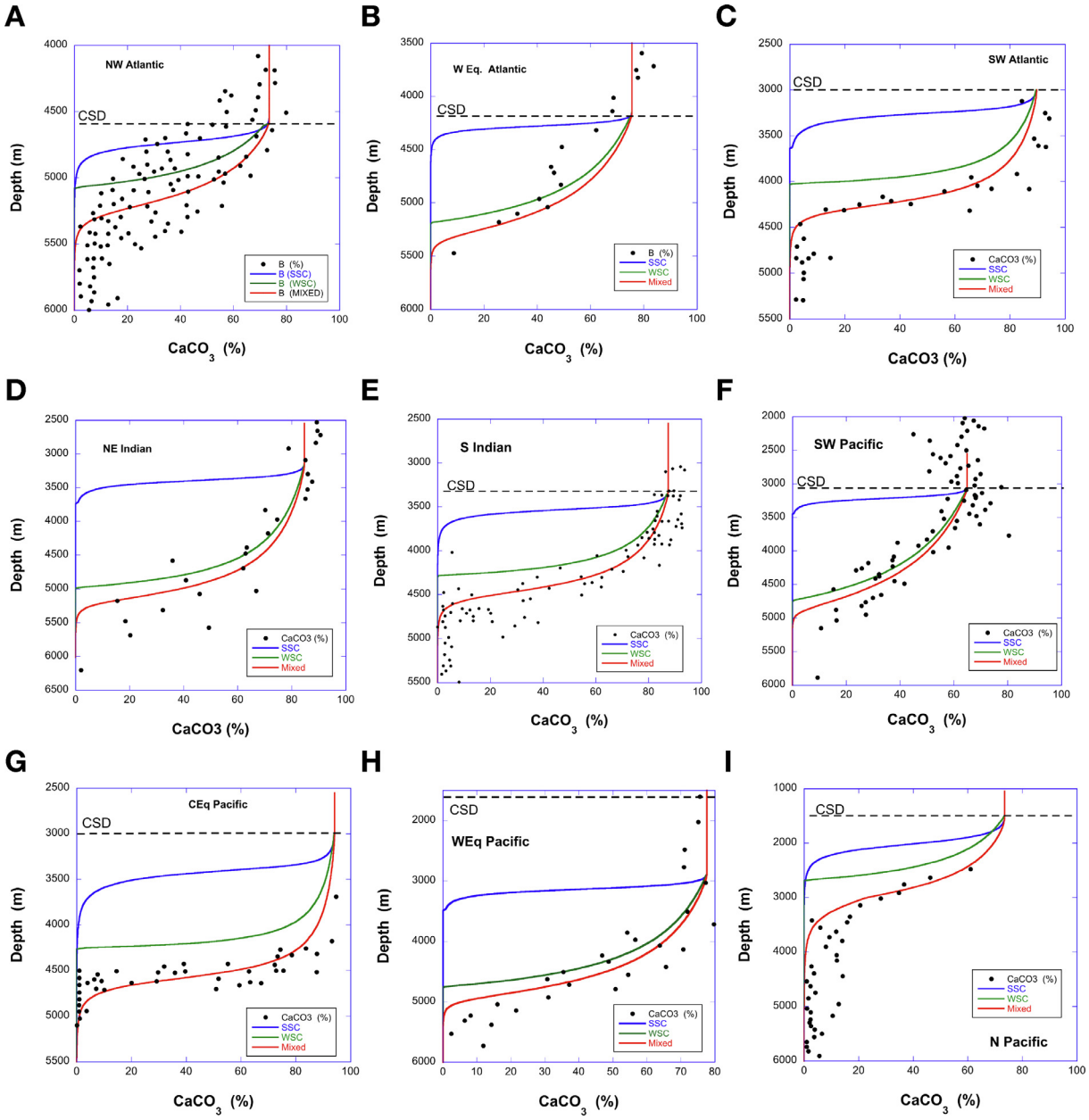

Fig. 5. Plots of predictions of the lysocline compared to data collected in 9 oceanic regions. The red curve is for transport-dominated (water-side) mixed control, the green curve represents pure water-side control of the dissolution, and the blue curve is pure sediment-side control, using the nonlinear kinetic formulation of Subhas et al. (2015) – see Eq. (1) of the text. The mixed control model represents nicely the observed data in each region, including the "tail". The pure water-side controlled model is an excellent approximation in 5 of the 9 cases. The pure sediment-side controlled model (blue) fails to represent any of the observed lysoclines.

vious sections. The k_h value in our calculations is that quoted for Eq. (1), corrected for temperature, as above, and $n = 4$.

The results of these computations for 9 regions are displayed in Fig. 5, in which each panel contains the reported $CaCO_3$ profile, either from Broecker and Peng (1982) or the database associated with Goff et al. (2008). Fig. 5 also illustrates the model predictions assuming mixed (red curves), pure water-side (green curves), and pure sediment-side (blue curves) control.

3.2. Discussion

In each case, a water-side-dominated, mixed-control model provides the best prediction of the lysocline, i.e., red lines in Fig. 5. The mixed model predicts the data trends in all cases, and it replicates the small tailing of the data at depth (Schink and Guinasso, 1977; Takahashi and Broecker, 1977). That tail is generated by the fact that as $B \to 0$, $k_c \to 0$, as per Eq. (5). (In natural sediments, tails can also be created by recalcitrant calcite particles.)

In 5 of the 9 cases in Fig. 5, the pure water-side controlled model (green lines) is visually close to the mixed-control lines (i.e., W Eq Atlantic, NE Indian, S Indian, SW Pacific, and W Eq Pacific), indicating that the rate is strongly influenced by the DBL mass-transfer rate. Hence, the water-side model constitutes an acceptable surrogate for the mixed model in many situations. The water-side model generates no tail at depth because the controlling rate parameter β in Eq. (3) is not dependent on B. Nevertheless, as argued by Boudreau (2013), very little of the accumulation of $CaCO_3$ in deep-sea sediments is contained within the tail (<3%), so that reproduction of this feature is not a crucial test of a control model.

On the other hand, prediction of lysoclines does constitute a crucial test, and a pure sediment-side control model (blue lines) fails to capture any of the lysoclines in Fig. 5. Given the results in Section 2 of this paper, this last observation is to be expected.

We can now unequivocally state that the Morse and Berner (1972) hypothesis that the sediment lysocline is a result of a nonlinear change in the rate of $CaCO_3$ dissolution with depth is untrue, if the Subhas et al. (2015) kinetic results are correct, which we believe is indeed the case. Furthermore, the Morse and Berner (1972) finding that transport (diffusion) is too fast to explain suspended $CaCO_3$ grain dissolution does not apply to the dissolution of sediment beds because the mass transport geometry and conditions are vastly different between these situations.

4. LINEAR VERSUS NONLINEAR DISSOLUTION KINETICS WITHIN THE SEAFLOOR

As explained in the Introduction, when one uses a rotating disc reactor, the apparent sediment-side kinetics are linear in the degree of undersaturation (Rickard and Sjöberg, 1983; Sulpis et al., 2017, 2019) in the limit of "high" rotation speeds (water-side limitation removed) – see Fig. 1. At the same time, suspended sediment dissolution clearly yields high-order nonlinearity e.g., $n = 4$ in Subhas et al. (2015) or a switch from $n \simeq 0.5$ to $n = 4.7$ in Naviaux et al. (2019a). Can that contradiction be resolved?

At least two possible explanations come to mind but there may be others. The first is that the kinetics of $CaCO_3$ dissolution change in a bed to become linear through some unknown mechanism. For example, inhibition that changes the order of reaction may occur in real sediments but not in the artificial beds; yet, the rate constant derived from Keir's (1983) experiment with real sediment plugs is essentially identical to that obtained by Sulpis et al. (2017) for artificial sediments. While inhibition in real sediments may still play a role, it does not seem to be the primary explanation for the apparent change in order.

A second explanation lies with a possible limitation of any bed-type reactor when relatively fast reactions occur near equilibrium, as in our case ($\Omega > 0.6$). The porewaters in the reactor will be very close to saturation, as demonstrated above. If we now perturb the overlying saturation state a bit to induce dissolution and thus measure the overall kinetics, the porewaters will rapidly re-adjust to try to attain saturation, and the exact kinetic response, linear versus nonlinear, may not be apparent within the sensitivity of the method because the response is fast. We emphasize that this suggested mechanism is entirely hypothetical.

On a more concrete level, Eq. (4) shows that the rotating disc will not indicate an $n = 4$ (Subhas et al., 2015) or $n = 0.5$ (Naviaux et al., 2019a) response to a change in $(1 - \Omega_\infty)$ but instead an order of $(n + 1)/2$, which is much closer to linear. No reactor design is perfect; yet, the rotating disc is the best simulator for the ocean bottom we presently have. If the second explanation above is valid, then predicted lysoclines with linear and nonlinear dissolution kinetics should be close to identical, and we explore that point next.

4.1. Results

Here, we wish to compare predicted lysoclines with nonlinear kinetics (Subhas et al., 2015), as given in Fig. 5 for water-side, mixed and sediment-side controls, with lysoclines predicted using linear dissolution kinetics within the bed, as generated by rotating-disk experiments at high rates of rotation (approximating the limit of $\omega \to \infty$), i.e., transport limitation largely removed. We note that rotating disc experiments produce values of k_s directly and not k_h. This latter fact is in no way a problem, as it is k_s we need for the flux balance, i.e., Eq. (7). This fact also eliminates the need to know the reactive surface area to convert k_h to k_s, as was done in Section 2 of this paper.

Assuming the Keir (1983) experiment is well mixed, i.e., no transport limitation, Boudreau (2013) extracted a maximum k_s of $\sim 1.12 \times 10^{-3}$ cm s^{-1} from that data. Similarly, Sulpis et al. (2017) obtained a k_s of $\sim 1.03 \times 10^{-3}$ cm s^{-1} as limit for high stirring velocities, which is essentially identical to the Keir-based value. In comparison, Rickard and Sjöberg (1983) obtain k_s values (which they call k_c) for Carrara marble and Iceland spar calcite of 2×10^{-2} and 6×10^{-3} cm s^{-1}, respectively. The rock $CaCO_3$ appears to be somewhat more reactive, but that may simply be the effect of a greater specific reactive surface area, rather than inherent reactivity. A typical value for k_s with linear dissolution kinetics is then chosen to be 1.0×10^{-3} cm s^{-1} at 20 °C.

Next, k_s is proportional to the square root of k_h – see Eq. (4); thus, we halve k_s rather than dividing it by 4, as done in Section 2 above, to correct k_s to in-situ temperature, i.e., $k_s \approx 5 \times 10^{-4}$ cm s^{-1} at 2 °C. Fig. 6 illustrates the predicted lysoclines for four oceanic regions generated with linear sediment-side reaction kinetics. (The other tested regions generate essentially the same types of plots.)

4.2. Discussion

Like the results in Fig. 5 with the nonlinear kinetics from Eq. (1), mixed (red lines) and water-side control (green lines) with linear dissolution kinetics correspond well to the $CaCO_3$ data in Fig. 6. Again, conversely, the sediment-side control predictions (blue lines) provide poor representations of that same data. Furthermore, the linear dissolution kinetic results are operationally identical to those with nonlinear kinetics given in Fig. 5, i.e., compare

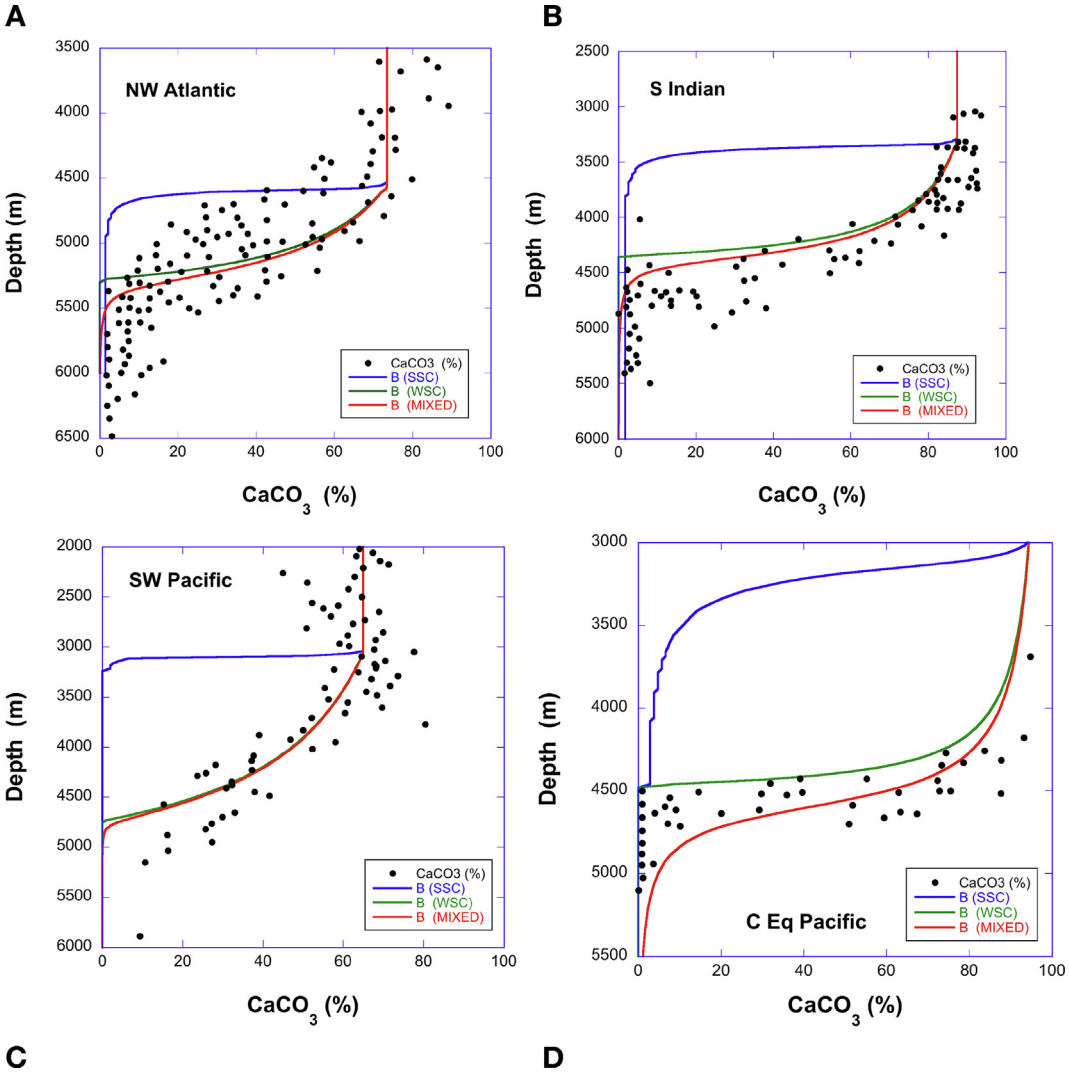

Fig. 6. Examples of the predictions of the lysoclines in 4 oceanic regions obtained with the linear sediment-side dissolution kinetics, derived from the rotating disc data of Sulpis et al. (2018, 2019). The data are mean profiles for these regions. The curves correspond to mixed control (red), sediment-side control (blue) and water-side control (green). Note that the sediment-side curve does not reproduce the observed data in any of these cases, nor for any other region we tested, while the mixed and water-side curves provide good approximations to the observations.

the same color lines in the corresponding panels in Figs. 5 and 6. The blue lines in Fig. 6 are essentially at the same depth positions as in Fig. 5, and the same is true of the red and green lines. This result means that there will be very little error in using linear kinetics to model benthic $CaCO_3$ dissolution in sediments, rather than the notionally more accurate nonlinear kinetics, and we take advantage of that conclusion in the next section. In addition, if one views the seafloor as a large bed reactor, then these results support our hypothesis that the order of a fast dissolution reaction will be difficult to ascertain in rotating-bed reactors.

5. PREDICTION OF POREWATER pH

As we stated earlier, prediction of the observed (in-situ) pH of deep-sea carbonate-bearing sediments has been treated sometimes as a test of our understanding of $CaCO_3$ dissolution, e.g., Archer (1991), Berelson et al. (1990, 1994), Jahnke et al. (1994, 1997), Martin and Sayles (1996), Hales and Emerson (1997), and Zeebe (2007). Diagenetic models that ignore DBL-effects need to adjust the dissolution rate constant to explain their data, which can only be done by assuming that the laboratory-determined rate constant is somehow altered in natural settings. No data has been provided that would explain the required reductions of up to two orders of magnitude. We show instead below that pH data can be predicted, not simply fit, if water-side (DBL) processes are included in a pH model, i.e., water-side-dominated mixed control.

Our diagenetic model for the dissolved carbonate system and pH in the porewaters of deep-sea sediments (see Table 1) is similar to that employed by Boudreau (1987), Archer et al. (1989) and Hales and Emerson (1996). Here, we assume that: (1) to simplify the solution of the model,

Table 1
Equations of the pH Model*.

(A) In the diffusive boundary layer (DBL):		
$D_1 C_1'' - R_c = 0$		(12)
$D_2 C_2'' + 2R_c = 0$		(13)
$D_3 C_3'' - R_c = 0$		(14)
$D_{Ca} C_{Ca}'' = 0$		(15)
(B) In the sediment porewater:		
$D_1/\theta^2\ C_1'' - R_c + \varepsilon R_{O2}\ e^{-\alpha x} = 0$		(16)
$D_2/\theta^2\ C_2'' + 2\ R_c = 0$		(17)
$D_3/\theta^2\ C_3'' - R_c + k_c\ (K_{sp} - C_{Ca}C_3) = 0$		(18)
$D_{Ca}/\theta^2\ C_C'' + k_c\ (K_{sp} - C_{Ca}C_3) = 0$		(19)
(C) Everywhere, equilibrium of dissolved carbonate solutes:		
$K_C = \frac{C_2^2}{C_1 C_3}$		(20)
Equilibrium hydrogen ion concentration in the porewater:		
$C_{H^+} = \sqrt{\frac{K_E C_1}{C_3}}$		(21)
(D) Boundary conditions:		
(i) known concentrations at the top of the DBL:		
$C_i = C_i^{\infty}$	$x = -\delta$	(22)
(ii) continuity of concentrations and diffusive fluxes at the sediment-water interface:		
$[C_i]_0^- = [C_i]_0^+$	$x = 0$	(23)
$[C_i']_0^- = [\varphi/\theta^2\ C_i']_0^+$	$x = 0$	(24)
(iii) Disappearance of gradients (fluxes) with great depth in the sediment:		
$C_i' \rightarrow 0$	$x \rightarrow \infty$	(25)

*Where:
x is depth.
i is an index for the solutes, i = 1 for CO_2(aq), i = 2 for bicarbonate ion, i = 3 for carbonate ion, i = Ca for calcium ion.
C_i is the concentration of species i.
D_i is the molecular/ionic diffusion coefficient of solute i (free solution).
θ^2 is the squared tortuosity.
φ is the mean porosity (0.8).
R_c is the rate of interconversion of dissolved carbonate species.
ε is the stoichiometric coefficient for the moles of CO_2 produced per mole of oxygen consumed in oxic organic matter decay.
α is a depth attenuation constant for CO_2 production by oxic organic matter decay.
R_{O2} is the rate of O_2 consumption by oxic organic matter decay at x = 0.
k_c is the (apparent) heterogeneous rate constant for calcite dissolution.
K_{sp} is the solubility product for calcite.
K_c is the quotient of the first and second stoichiometric dissociation constants for carbonic acid in seawater.
K_E is the product of the first and second stoichiometric dissociation constants for carbonic acid in seawater.
$[\ ]_0-$ indicates the value of a quantity on the water side of x = 0.
$[\ ]_0+$ indicates the value of a quantity on the sediment side of x = 0.
C_i' indicates a first spatial (depth) derivative of the concentration of species i.
C_i'' indicates a second spatial (depth) derivative.

we employ linear dissolution kinetics, with the experimentally-determined rate constants of Section 4.1; (2) besides calcite dissolution, only oxic organic matter decay is assumed to occur, and this reaction can be represented as an exponentially decreasing source function for CO_2; thus, sub-oxic diagenesis is ignored; (3) porosity is treated as a mean constant value, i.e., 0.8; (4) steady state and uni-dimensionality are assumed; (5) the dissolved carbonate species are assumed to be in thermodynamic equilibrium at all depths; (6) porewater advection, due to burial and compaction, and porewater bioturbation and irrigation are ignored; (7) there is a diffusive sublayer on the waterside of the sediment-water interface of thickness δ; (8) the calcite in the sediment is considered well mixed; (9) any cross coupling with other solutes (Boudreau et al., 2004) is ignored; and finally, (10) the hydrogen ion is in equilibrium with the carbonate system. Neglecting porosity gradients near the sediment-water interface, where they are strongest, may seem questionable, but if the porewaters are essentially at calcite equilibrium, the implied changes in calcite content have little effect, and the changes to the diffusion coefficients are modest. With these assumptions, an (approximate) analytical solution is possible (see the SI for details about the solution). The FORTRAN code for this solution is also contained in the SI.

To investigate the capability of this model to predict observed porewater pH profiles, the constants in the equations in Table 1 are preset and not used as free parameters to fit the data. In particular, the diffusion coefficients are calculated with the equations in Boudreau (1997); the tortu-

osity from the mean observed porosity (Boudreau, 1996); the CO_2 production ratio ε (β in Hales and Emerson, 1996; not to be confused with our water-side mass-transfer coefficient) was taken as the Redfield value of 0.77; the stoichiometric solubility product of calcite at 1 atmosphere at 25 °C (K^*_{sp}) was obtained from Mucci (1983), while corrections for the value at in-situ temperature and pressure were obtained from Millero (1983); stoichiometric constants for the carbonic acid first and second dissociation reactions were obtained from Millero (1995), Clegg and Whitfield (1995), with corrections for pressure effects from Millero (1983) and UNESCO (1983); the DBL thickness (δ) was set to an ocean wide mean value of 1 mm (Boudreau, 2001; Boudreau, 2013).

Finally, we needed to set the linear rate constant for calcite dissolution in the sediment, k_c in our equations. Past experiments by Keir (1983), as re-interpreted by Boudreau (2013), and new experiments by Sulpis et al. (2017) provide values of the sediment-side mass-transfer coefficient, k_s, and this composite parameter is related to k_c via Eq. (8). Knowing k_s from experiments, we can invert this value for k_c, with the specific reactive surface area noted in Section 4. This inversion is entirely formal as the solution method turns it back into k_s, which is an observed value. The experiments for k_s were not conducted at seafloor temperatures (or pressures), but this does not truly affect our findings – see Part 4 of the SI.

5.1. Results

The O_2 and pH data used in this study originate from Archer et al. (1989), i.e., their Stations 13 and 14 in the Central Equatorial Atlantic, and Hales and Emerson (1996), i.e., their stations 2A and 2B on the Ontong-Java Plateau – see Table 2 for relevant input data for these stations. Station 3 data are not used because the amount of calcite in the sediment is not consistent with the reported saturation state of the overlying waters when compared to the other Ontong-Java sites, i.e., at $\Omega = 0.91$, Station 2 reports 90% $CaCO_3$, while Station 3 at $\Omega = 0.75$ reports 90% $CaCO_3$, which is not possible at steady state and assuming similar sedimentation rates. Station 3 is also anomalous compared to the Atlantic stations, which also have essentially the same degree of undersaturation. When used in the model, the trend in the Station 3 data is replicated, but the absolute pH value is 0.2 unit higher. We thus chose not to use these data. Sediments from these stations all come from below the calcite saturation depth ($\Omega_\infty < 1$) under in-situ T, S and P conditions. Finally, single exponential fits to the O_2 data at these stations, from which the model parameters α, a depth attenuation constant for CO_2 metabolic production and R_{O2}, the rate of metabolic O_2 consumption, are illustrated in Part 4 of the SI.

Fig. 7 illustrates the ΔpH data from the four stations noted above. ΔpH is the difference between the measured pH and the pH in the bottom waters, which is the convention used in Hales and Emerson (1996). Archer et al. (1989) calculate, δpH, which is the additive inverse (or negation) of ΔpH. The choice of the convention is entirely arbitrary, but we prefer that higher relative pH values be positive quantities. The observational data were reported by the original studies in this manner because of uncertainty in the absolute values of pH. The data are plotted with their original symbols for easier reference. The red line is the model prediction in each case; no parameter was varied or adjusted within the model to achieve these results.

5.2. Discussion

Overall, the correspondence between one of the data trends in each plot and the model is visually good (no quantitative measure). At Stations 13 and 14 in the Atlantic, the model predictions follow the increasing trend in the data, given as plus signs and solid squares, reasonably closely and contain a maximum at about 0.05 cm, which also appears in the data. In these sediments, calcite dissolution overwhelms the acidification from oxic organic matter decay and causes the porewaters to alkalinize. In contrast, at Stations 2A and 2B, the models capture the initial fall in ΔpH but deviates from the data at depth, more so at Station 2A. ΔpH is negative at these stations, indicating a dominance of CO_2 release in the porewaters from oxic organic matter decay (Emerson and Bender, 1982). The deviations further indicate that suboxic diagenetic reactions, i.e., dissolved nitrate and solid manganese and iron oxide reductions, raise the pH at depth as they produce bicarbonate ions, i.e., alkalinity. We do not suggest that these suboxic reactions (necessarily) occur in the oxic zone; only that their bicarbonate metabolic product diffuses up into that layer. These suboxic reactions are not included in our model but the predicted near-surface pH changes are certainly consistent with the observations. Suboxic diagenesis influ-

Table 2
Parameters for the selected data sites as obtained from Archer et al. (1989) and Hales and Emerson (1996).

Site	Depth (m)	Salinity	Temp. (°C)	ΣCO_2 (μM)	Total Alkalinity (μM)*	Overlying water calcite saturation Ω_c	% Calcite in sediment $X_{calcite}$
13	4950	34.8	2.5	2250	2365	0.76	8–10
14	5075	34.8	2.5	2250	2365	0.74	8–10
2A	2322	34.6	2.0	2345	2404	0.91	~90
2B	2335	34.6	2.0	2345	2404	0.91	~90

* Carbonate alkalinity is calculated by correcting for borate alkalinity.

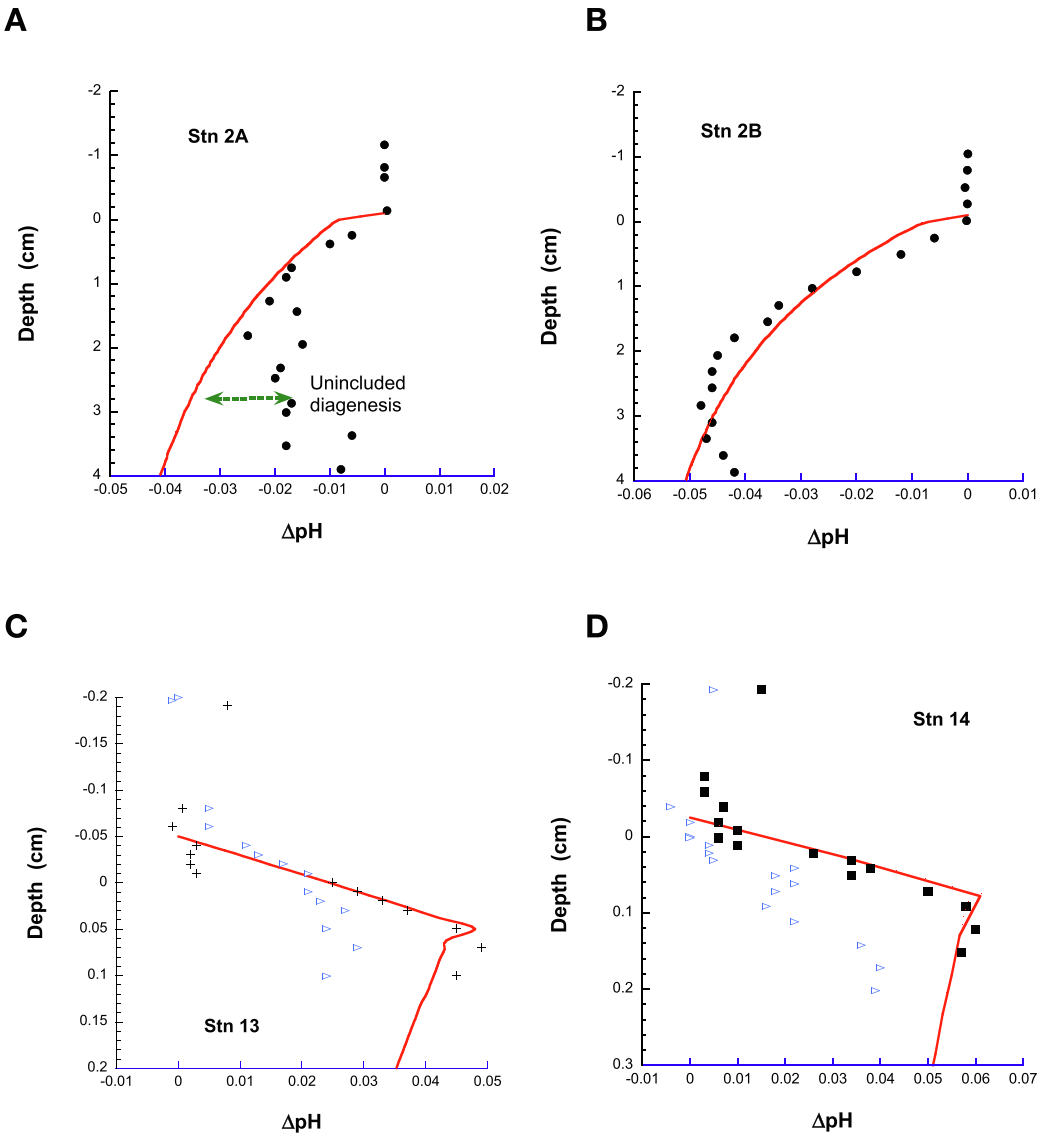

Fig. 7. Comparison between the ΔpH data and the predictions from a model based on laboratory-derived calcite dissolution rates and overall water-side mass transfer control developed in the present paper (Table 1). Panels A and B are the data from the Ontong-Java Plateau (Hales and Emerson, 1996) and Panels C and D are data from the Central Atlantic Ocean (Archer et al., 1989). Data are plotted with their original symbols, so as to facilitate comparison with the figures in the original references. NOTE: The positional accuracy of the Archer et al. (1989) profiles is no better than ±0.1 cm. In other words, the sediment-water interface position in these data is only 0 ± 0.1 cm and could be as much as 0.1 cm above where it is reported or 0.1 cm deeper. We struggled with this problem of positional inaccuracy and came to the conclusion that the linearity of the pH profiles better suggested that the true sediment-water interface was actually about 0.05 cm deeper at both stations than reported. Thus, the DBL really extended from about −0.05 cm to +0.05 cm. The break in the pH profile at +0.05 cm is consistent with the location of the start of CO_2 addition in the sediment, i.e., the sediment-water interface. Thus, while we display the results with Archer et al. (1989) positions, the computations were done with a −0.05 cm shifted axis.

ence in cores with much lower interfacial/bottom-water oxygen or higher organic carbon accumulation rates is to be expected.

Our model predicts pH variations, as can be seen in Fig. 7, even though the porewaters are at equilibrium with calcite. Why? To answer, consider the two dissociation reactions for carbonic acid in seawater:

$$CO_2(aq) + H_2O \leftrightarrow HCO_3^- + H^+$$

$$HCO_3^- \leftrightarrow CO_3^{2-} + H^+$$

If we add these two reactions, we obtain a single reaction involving the hydrogen ion and two carbonate species,

$$CO_2(aq) + H_2O \leftrightarrow CO_3^{2-} + 2H^+$$

Assuming equilibrium of the dissolved carbonate species, the mass-action law for this third reaction is

$$K_E = \frac{C_3 C_{H^+}^2}{C_1} \tag{26}$$

where C_1 is the concentration of CO_2(aq), C_3 is the concentration of the carbonate ion, C_H^+ is the hydrogen-ion concentration, and K_E is a stoichiometric equilibrium constant. K_E equals the product of the equilibrium constants for the first and second reactions listed above. Rearrangement of this last equation gives Eq. (21) of Table 1,

$$C_{H^+} = \sqrt{\frac{K_E C_1}{C_3}} \tag{21, repeated}$$

If the carbonate-ion concentration is at equilibrium with calcite, and thus equal to the saturation value, i.e., $C_3 = C_s$ in this equation, both the porewater CO_2 concentration, C_1, and the hydrogen ion concentration, C_H^+, are free to vary in accordance with Eq. (21). Consequently, if oxic organic matter decay generates dissolved porewater CO_2, thus increasing C_1 with depth into the sediment, then C_{H+} will rise (as a square root function) and pH will fall, even if C_3 is fixed. Equilibrium with calcite does not negate the existence of pH gradients.

6. SUMMARY OF FINDINGS

Firstly, we advance that the kinetic rate constant for calcite dissolution determined in laboratory studies, such as in Subhas et al. (2015), apply to the sediment bed of the deep-sea and cannot be manipulated unjustifiably to smaller values. Given this proposition, it is then possible to compare quantitatively the speed of sediment-side supply of dissolved carbonate ions, k_s, with their water-side transfer speed through the diffusive boundary layer (DBL), β, i.e., the ratio k_s/β. This comparison reveals that the value k_s/β in the deep-ocean floor is always much larger than unity (typically 100–750), thus establishing that the speed of the carbonate ion transfer across the DBL dominates the control of calcite dissolution at the deep seafloor (Fig. 3). Consequently, sediment porewaters near the SWI are largely at or close to saturation with respect to calcite (Fig. 4). These findings falsify the long-held idea, first proposed by Morse and Berner (1972), that the observed kinetic control of dissolving suspended spheres applies to the dissolution of a $CaCO_3$-bearing seabed.

Secondly, we show that observed lysoclines are well reproduced by a water-side dominated mixed-control model (Fig. 5), i.e., the sediment-side processes only become important near the CCD (as $B \to 0$). A model that is sediment-side controlled and uses the nonlinear Subhas et al. (2015) rates, i.e., no DBL resistance, fails to reproduce any observed lysoclines.

Thirdly, rotating disc dissolution experiments most likely display linear dissolution with respect to undersaturation, $1 - \Omega$ (Rickard and Sjöberg, 1983; Sulpis et al., 2018, 2019) because the device is not sensitive to the order of reaction for a very fast reaction close to equilibrium. In contrast, suspended grain experiments are sensitive to the order, even if they do not simulate seabed dissolution. Nevertheless, model results predicting $CaCO_3$-depth profiles in the ocean (lysoclines) are almost identical using either the nonlinear kinetics for dissolution (Fig. 5) or the linear kinetics (Fig. 6). Thus, nonlinearity is not a vital aspect in quantitatively describing seafloor dissolution, and linear kinetics can be adopted when needed.

Fourthly, we illustrate that a model based on the observed fast dissolution kinetics for calcite beds (Sulpis et al., 2017, 2019) leads to reasonable *predictions* of observed *pH*-depth profiles in oceanic porewaters, i.e., no parameter adjustment – see Fig. 7. Consequently, our theory that calcite dissolution at the deep seafloor is mainly water-side mass-transfer controlled (Boudreau et al., 2010a; Boudreau, 2013; Sulpis et al., 2017, 2019) passes a strong test to its validity.

ACKNOWLEDGEMENTS

This research was funded in part by a Natural Sciences and Engineering Research Council Discovery grant to AM (RGPIN/04421-2018). BPB was supported by funds from the Killam Trust and Dalhousie University. OS also acknowledges the Dept. of Earth and Planetary Sciences at McGill University for financial support, including the Lynch and McGregor scholarships, during his residency in the graduate program. Chris Jenkins is thanked for access to his database. Finally, we wish to thank the three journal reviewers, including Adams Subhas, and Associate Editor Robert Byrne for critical comments on previous versions of this manuscript.

APPENDIX A. SUPPLEMENTARY MATERIAL

Supplementary data to this article can be found online at https://doi.org/10.1016/j.gca.2019.09.037.

REFERENCES

Arakaki T. and Mucci A. (1995) A continuous and mechanistic representation of calcite reaction-controlled kinetics in dilute solutions at 25°C and 1 atm total pressure. *Aquat. Geochem.* **1**, 105–130. https://doi.org/10.1007/BF01025233.

Archer D. E. (1991a) Equatorial Pacific calcite preservation cycles: production or dissolution? *Paleoceanogr.* **6**, 561–571.

Archer D. E. (1991b) Modeling the calcite lysocline. *J. Geophys. Res.* **96**, 17037–17050.

Archer D. E., Emerson S. and Reimers C. (1989) Dissolution of calcite in deep-sea sediments: pH and O_2 microelectrode results. *Geochim. Cosmochim. Acta* **53**, 2831–2845. https://doi.org/10.1016/0016-7037(89)90161-0.

Berelson W. M., Hammond D. E., McManus J. and Kilgore T. E. (1994) Dissolution kinetics of calcium carbonate in equatorial Pacific sediments. *Global Biogeochem. Cycles* **8**, 219–235.

Berelson W. M., Hammond D. E. and Cutter G. A. (1990) *In situ* measurements of calcium carbonate dissolution rates in deep-sea sediments. *Geochim. Cosmochim. Acta* **54**, 3013–3020.

Berger W. H. (1967) Foraminiferal ooze: solution at depth. *Science* **156**, 83–85.

Berger W. H. (1968) Planktonic foraminifera: selective solution and the lysocline. *Mar. Geol.* **15**, 31–43.

Berner R. A. (1978) Rate control of mineral dissolution under earth surface conditions. *Amer. J. Sci.* **278**, 1235–1252.

Berner R. A. (1980) *Early Diagenesis: A Theoretical Approach*. Princeton Univ. Press, Princeton, NJ, USA, p. 241.

Berner R. A. and Morse J. W. (1974) Dissolution kinetics of calcium carbonate in sea water: IV. Theory of calcite dissolution. *Amer. J. Sci.* **274**, 108–134.

Boudreau B. P. and Luo Y. (2017) Retrodiction of secular variations in deep-sea $CaCO_3$ burial during the Cenozoic. *Earth Planet. Sci.* **474**, 1–12.

Boudreau B. P. (1987) A steady-state diagenetic model for dissolved carbonate species and pH in porewaters of oxic and suboxic sediments. *Geochim. Cosmochim. Acta* **51**, 1985–1996.

Boudreau B. P. (1996) The diffusive tortuosity of fine-grained unlithified sediments. *Geochim. Cosmochim. Acta* **60**, 3139–3142.

Boudreau B. P. (1997) Diagenetic Models and their Implementation, Springer-Verlag, Berlin. 417p. Note: This book is in the public domain and a copy can be obtained from the website: <https://www.researchgate.net/publication/235335761_Diagenetic_models_and_their_implementation_modelling_transport_and_reactions_in_aquatic_sediments>.

Boudreau B. P. (2001) Solute transport above the sediment-water interface. In *The Benthic Boundary Layer: Transport Processes and Biogeochemistry* (eds. B. P. Boudreau and B. B. Jørgensen). Oxford Univ. Press, Oxford, U.K., pp. 104–126.

Boudreau B. P. (2013) Carbonate dissolution rates at the deep ocean floor. *Geophys. Res. Lett.* **40**, 1–5. https://doi.org/10.1029/2012GL054231.

Boudreau B. P. and Guinasso Jr. N. L. (1982) The influence of a diffusive sublayer on accretion, dissolution, and diagenesis at the sea floor. In The Dynamic Environment of the Ocean Floor, (eds. K.A. Fanning and F.T. Manheim), Lexington Books, Lexington, MA, USA, pp. 115–145. Note: This chapter is in the public domain and a copy can be obtained from the website: <https://www.researchgate.net/publication/236670208_The_Influence_of_a_Diffusive_Sublayer_on_Accretion_Dissolution_and_Diagenesis_at_the_Sea_Floor>.

Boudreau B. P. and Jørgensen B. B. (2001) *The Benthic Boundary Layer: Transport Processes and Biogeochemistry*. Oxford Univ. Press, Oxford, U.K., p. 404.

Boudreau B. P., Meysman F. J. R. and Middelburg J. J. (2004) Multicomponent ionic diffusion in porewaters: Coulombic effects revisited. *Earth Planet. Sci. Lett.* **222**, 653–666. https://doi.org/10.1016/j.epsl.2004.02.034.

Boudreau B. P., Middelburg J. J. and Luo Y. (2018) The role of calcification in carbonate compensation. *Nat. Geosci.* **11**, 894–900. https://doi.org/10.1038/s41561-018-0259-5.

Boudreau B. P., Middelburg J. J. and Meysman F. J. R. (2010a) Carbonate compensation dynamics. *Geophys. Res. Lett.* **37**, L03603. https://doi.org/10.1029/2009GL041847.

Boudreau B. P., Middelburg J. J., Hofmann A. F. and Meysman F. J. R. (2010b) Ongoing transients in carbonate compensation. *Global Biogeochem. Cycles* **24**, GB4010. https://doi.org/10.1029/2009GB003654.

Broecker W. S. and Peng T.-H. (1982) *Tracers in the Sea*. Eldigio, Palisades, NY, p. 690.

Burdige D. J. (2006) *Geochemistry of Marine Sediments*. Princeton Univ. Press, Princeton, p. 609.

Caves J. K., Jost A. B., Lau K. V. and Maher K. (2016) Cenozoic carbon cycle imbalances and a variable weathering feedback. *Earth Planet. Sci. Lett.* **450**, 152–163. https://doi.org/10.1016/j.epsl.2016.06.035.

Clegg S. L. and Whitfield M. (1995) A chemical model of seawater including dissolved ammonia and the stoichiometric dissociation constant of ammonia in estuarine water and seawater from −2 to 40°C. *Geochim. Cosmochim. Acta* **59**, 2403–2421. https://doi.org/10.1016/0016-7037(95)00135-2.

Dickson A. G. (1990) Standard potential of the reaction: AgCl(s) +1/2H2(g) = Ag(s)+HCl(aq), and the standard acidity constant of the ion HSO_4^- in synthetic sea water from 273.15 to 318.15 K. *J. Chem. Thermodyn.* **22**, 113–127.

Dong S., Subhas A. V., Rollins N. E., Naviaux J. D., Adkins J. F. and Berelson W. M. (2018) A kinetic pressure effect on calcite dissolution in seawater. *Geochim. Cosmochim. Acta* **238**, 411–423.

Emerson S. and Bender M. (1982) Carbon fluxes at the sediment-water interface of the deep-sea: calcium carbonate preservation. *J. Mar. Res.* **39**, 139–162.

Gehlen M., Bassinot F. C., Chou L. and McCorkle D. (2005a) Reassessing the dissolution of marine carbonates: II. Reaction kinetics. *Deep-Sea Res. I* **52**, 1461–1476.

Gehlen M., Bassinot F. C., Chou L. and McCorkle D. (2005b) Reassessing the dissolution of marine carbonates: I. Solubility. *Deep-Sea Res. I* **52**, 1445–1460.

Gledhill D. K. and Morse J. W. (2006) Calcite dissolution kinetics in Na-Ca-Mg-Cl brines. *Geochim. Cosmochim. Acta* **70**, 5802–5813.

Goff J. A., Jenkins C. J. and Williams S. J. (2008) Seabed mapping and characterization of sediment variability using the usSEABED data base. *Cont. Shelf Res.* **28**, 614–633.

Hales B. and Emerson S. (1996) Calcite dissolution in sediments of the Ontong-Java Plateau: in situ measurements of pore water O_2 and pH. *Global Biogeochem. Cycles* **10**, 527–541.

Hales B. and Emerson S. (1997) Evidence in support of first-order dissolution kinetics of calcite in seawater. *Earth Planet. Sci. Lett.* **148**, 317–327. https://doi.org/10.1016/S0012-821X(97)00017-4.

Jahnke R. A., Craven D. B. and Gaillard J.-F. (1994) The influence of organic matter diagenesis on $CaCO_3$ dissolution at the deep-sea floor. *Geochim. Cosmochim. Acta* **58**, 2799–2809. https://doi.org/10.1016/0016-7037(94)90115-5.

Jahnke R. A., Craven D. B., McCorkle D. C. and Reimers C. E. (1997) $CaCO_3$ dissolution in California continental margin sediments: the influence of organic matter remineralization. *Geochim. Cosmochim. Acta* **61**, 3587–3604.

Jenkin C. J. (1997) Building offshore soils databases. *Sea Technology* **38**(12), 25–28.

Keir R. S. (1980) The dissolution kinetics of biogenic calcium carbonates in seawater. *Geochim. Cosmochim. Acta* **44**, 241–252. https://doi.org/10.1016/0016-7037(80)90135-0.

Keir R. S. (1982) Dissolution of calcite in the deep-sea: theoretical prediction for the case of uniform size particles settling into a well-mixed sediment. *Am. J. Sci.* **282**, 193–236.

Keir R. S. (1983) Variation in the carbonate reactivity of deep-sea sediments: determination from flux experiments. *Deep Sea Res. Part A* **30**, 279–296. https://doi.org/10.1016/0198-0149(83)90011-0.

Key R. M., Olsen A., van Heuven S., Lauvset S. K., Velo A., Lin X., Schirnick C., Kozyr A., Tanhua T., Hoppema M., Jutterström S., Steinfeldt R., Jeansson E., Ishi M., Perez F. F. and Suzuk, T. (2015) Global Ocean Data Analysis Project, Version 2 (GLODAPv2), ORNL/CDIAC-162, NDP-P093. Carbon Dioxide Information Analysis Center, Oak Ridge National Laboratory, US Department of Energy, Oak Ridge, Tennessee.

Kennett J. P. (1982) *Marine Geology*. Prentice-Hall, Englewood Cliffs, NJ, USA, p. 813.

Kump L. R., Bralower T. J. and Ridgwell A. (2009) Ocean acidification in deep time. *Oceanography* **22**, 94–107.

Levich V. G. (1962) *Physicochemical Hydrodynamics*. Prentice-Hall Inc., Englewood Cliffs, p. 700.

Lewis E. and Wallace D. W. R. (1998) *Program Developed for CO_2 System Calculations, ORNL/CDIAC-105*. Anal. Cent., Oak Ridge Natl. Lab., Oak Ridge, Tenn, Carbon Dioxide Inf, p. 38.

Lueker T. J., Dickson A. G. and Keeling C. D. (2000) Ocean pCO_2 calculated from dissolved inorganic carbon, alkalinity, and equations for K_1 and K_2: validation based on laboratory

measurements of CO_2 in gas and seawater at equilibrium. *Mar. Chem.* **70**, 105–119.

Maldonado C. F. E., Giroir G., Dandurand J. L. and Schott J. (1992) The dissolution of calcite in seawater from 40°C to 90°C at atmospheric pressure and 35 $^{o}/_{oo}$ salinity. *Chem. Geol.* **97**, 113–123.

Martin W. R. and Sayles F. L. (1996) $CaCO_3$ dissolution in sediments of the Ceara Rise, western equatorial Atlantic. *Geochim. Cosmochim. Acta* **60**, 243–263.

Millero F. J. (1983) The effect of pressure on the solubility of minerals in water and seawater. *Geochim. Cosmochim. Acta* **41**, 11–22.

Millero F. (1995) Thermodynamics of the carbon dioxide system in the oceans. *Geochim. Cosmochim. Acta* **59**, 661–677.

Millero F. J. (2007) The marine inorganic carbon cycle. *Chem. Rev.* **107**, 308–341.

Morse J. W. (1974) Calculation of diffusive fluxes across the sediment-water interface. *J. Geophys. Res.* **33**, 5045–5048.

Morse J. W. (1978) Dissolution kinetics of calcium carbonate in sea water: VI. The near-equilibrium dissolution kinetics of calcium carbonate-rich deep-sea sediments. *Am. J. Sci.* **278**, 344–353.

Morse J. W. (2005) Formation and diagenesis of carbonate sediments. In *Sediments, Diagenesis, and Sedimentary Rocks* (ed. F. T. Mackenzie). Elsevier, Amsterdam, pp. 67–86.

Morse J. W. and Arvidson R. S. (2002) The dissolution kinetics of major sedimentary carbonate minerals. *Earth-Sci. Rev.* **58**, 51–84.

Morse J. and Berner R. A. (1972) Dissolution of calcium carbonate in sea water: II. A kinetic origin of the lysocline. *Amer. J. Sci.* **272**, 840–851.

Mucci A. (1983) The solubility of calcite and aragonite in seawater at various salinities, temperatures and one atmosphere total pressure. *Amer. J. Sci.* **283**, 780–799.

Naviaux J. D., Subhas A. V., Dong S., Rollins N. E., Liu X., Byrne R. H., Berelson W. M. and Adkins J. K. (2019a) Calcite dissolution rates in seawater: lab vs. in-situ measurements and inhibition by organic matter. *Mar. Chem.* **215** 103684.

Naviaux J. D., Subhas A. V., Rollins N. E., Dong S., Berelson W. M. and Adkins J. F. (2019b) Temperature dependence of calcite dissolution kinetics in seawater. *Geochim. Cosmochim. Acta* **246**, 363–384.

Olsen A., Key R. M., van Heuven S., Lauvset S. K., Velo A., Lin X., Schirnick C., Kozyr A., Tanhua T., Hoppema M., Jutterströ S., Steinfeldt R., Jeansson E., Ishii M., Pérez F. F. and Suzuki T. (2016) The Global Ocean Data Analysis Project version 2 (GLODAPv2) – an internally consistent data product for the world ocean. *Earth Syst. Sci. Data* **8**, 297–323.

Peterson M. N. A. (1966) Calcite: rates of dissolution in a vertical profile in the Central Pacific. *Science* **154**, 1542–1544.

Pytkowicz R. M. (1970) On the carbonate compensation depth in the Pacific Ocean. *Geochim. Cosmochim. Acta* **34**, 836–839.

Raimondi L., Matthews J. B. R., Atamanchuck D., Azetsu-Scott K. and Wallace D. (2019) The internal consistency of the marine carbon dioxide system for high latitude shipboard and in situ monitoring. *Mar. Chem.* **213**, 49–70. https://doi.org/10.1016/j.marchem.2019.03.001.

Rickard D. and Sjöberg E. L. (1983) Mixed kinetic control of calcite dissolution rates. *Amer. J. Sci.* **283**, 815–830.

Santschi P. H., Anderson R. F., Fleisher M. Q. and Bowles W. (1991) Measurements of diffusive sublayer thicknesses in the ocean by alabaster dissolution, and their implications for the measurements of benthic fluxes. *J. Geophys. Res.* **96**, 10641–10657.

Sarmiento J. J. and Gruber N. (2006) *Ocean Biogeochemical Dynamics*. Princeton Univ. Press, Princeton, p. 503.

Schink D. R. and Guinasso, Jr., N. L. (1977) Modeling the onfluence of bioturbation and other processes on carbonate dissolution on the sea floor. In *The Fate of Fossil Fuel CO_2 in the Oceans* (eds. N. R. Anderson and A. Malahoff). Plenum, New York, pp. 375–399.

Sjöberg E. L. and Rickard D. (1983) The influence of experimental design on the rate of calcite dissolution. *Geochim. Cosmochim. Acta* **47**, 2281–2285.

Sjöberg E. L. and Rickard D. (1984a) Calcite dissolution kinetics: surface speciation and the origin of the variable pH dependence. *Chem. Geol.* **42**, 119–136.

Sjöberg E. L. and Rickard D. (1984b) Temperature dependence of calcite dissolution kinetics between 1 and 62°C at pH 2.7 to 8.4 in aqueous solutions. *Geochim. Cosmochim. Acta* **48**, 485–493.

Subhas A. V., Rollins N. E., Berelson W. M., Dong S., Erez J. and Adkins J. F. (2015) A novel determination of calcite dissolution kinetics in seawater. *Geochim. Cosmochim. Acta* **170**, 51–68.

Sulpis O., Boudreau B. P., Mucci A., Jenkins C., Trossman D. S., Arbic B. K. and Key R. M. (2018) Current $CaCO_3$ dissolution at the seafloor caused by anthropogenic CO_2. *Proc. Nat. Acad. Sci.* **115**, 11700–11705.

Sulpis O., Lix C., Mucci A. and Boudreau B. P. (2017) Calcite dissolution kinetics at the sediment-water interface in natural seawater. *Mar. Chem.* **195**, 70–83.

Sulpis O., Mucci A., Boudreau B. P., Barry M. and Johnson B. (2019) Controlling the diffusive boundary layer thickness above the sediment-water interface in a thermostated, rotating-disk reactor. *Limnol. Oceanogr. Methods* **17**, 241–253. https://doi.org/10.1002/lom3.10309.

Takahashi T. and Broecker W. S. (1977) Mechanisms for calcite dissolution on the sea floor. In *The Fate of Fossil Fuel CO2 in the Oceans* (eds. N. R. Anderson and A. Malahoff). Plenum, New York, pp. 455–477.

Tyrrell T. and Zeebe R. E. (2004) History of carbonate ion concentration over the last 100 million years. *Geochim. Cosmochim. Acta* **68**, 3521–3530.

UNESCO (1983) Carbon dioxide sub-group of the joint panel on oceanographic tables and standards. Tech. Papers Marine Science 42, Paris, France.

van Heuven S., Pierrot D., Rae J. W. B., Lewis E., Wallace D. W. R. (2011) MATLAB program developed for CO_2 system calculations, ORNL/CDIAC-105b, Carbon Dioxide Inf. Anal. Cent., Oak Ridge Natl. Lab., US DOE, Oak Ridge, Tenn.

Zachos J. C., Röhl U., Schellenberg S. A., Sluijs A., Hodell D. A., Kelly D. C., Thomas E., Nicolo M., Raffi I., Lourens L. J., McCarren H. and Kroon D. (2005) Rapid acidification of the ocean during the Paleocene-Eocene Thermal Maximum. *Science* **308**, 1611–1615.

Zeebe R. E. (2007) Modeling CO_2 chemistry, $\delta^{13}C$, and oxidation of organic carbon and methane in sediment porewater: implications for paleo-proxies in benthic foraminifera. *Geochim. Cosmochim. Acta* **71**, 3238–3256. https://doi.org/10.1016/j.gca.2007.05.004.

Zeebe R. E. (2012) LOSCAR: Long-term Ocean-atmosphere-sediment Carbon cycle reservoir model v2.0.4. *Geosci. Model. Dev.* **5**, 149–166.

Zeebe R. E. and Tyrrell T. (2019) History of carbonate ion concentration over the last 100 million years II: revised calculations and new data. *Geochim. Cosmochim. Acta* **257**, 373–392. https://doi.org/10.1016/j.gca.2019.02.041.

Associate editor: Robert H. Byrne